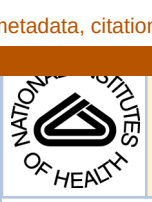

Published in final edited form as:
Nat Neurosci. ; 15(4): 620–627. doi:10.1038/nn.3047.

A cortical motor nucleus drives the basal ganglia-recipient thalamus in singing birds

Jesse H. Goldberg and **Michale S. Fee**
McGovern Institute for Brain Research, Department of Brain and Cognitive Sciences, Massachusetts Institute of Technology, MIT 46-5133, 77 Massachusetts Avenue, Cambridge, MA 02139

Michale S. Fee: fee@mit.edu

Abstract

The pallido-recipient thalamus transmits information from the basal ganglia (BG) to the cortex and plays a critical role motor initiation and learning. Thalamic activity is strongly inhibited by pallidal inputs from the BG, but the role of non-pallidal inputs, such as excitatory inputs from cortex, is unclear. We have recorded simultaneously from presynaptic pallidal axon terminals and postsynaptic thalamocortical neurons in a BG-recipient thalamic nucleus necessary for vocal variability and learning in zebra finches. We found that song-locked rate modulations in the thalamus could not be explained by pallidal inputs alone, and persisted following pallidal lesion. Instead, thalamic activity was likely driven by inputs from a motor 'cortical' nucleus also necessary for singing. These findings suggest a role for cortical inputs to the pallido-recipient thalamus in driving premotor signals important for exploratory behavior and learning.

Basal ganglia (BG) thalamocortical circuits are evolutionarily conserved among vertebrates and widely implicated in motor control and learning[1, 2]. The major output of the BG circuit —pallidal neurons that are GABAergic and tonically active—are thought to control movements by inhibiting or disinhibiting their targets in the pallido-recipient thalamus[3-5]. This thalamic area also receives excitatory inputs from cortex[6], but thalamic integration of cortical and pallidal inputs is poorly understood. In human disease, the pallidal inputs are often emphasized: insufficient pallidal inhibition of thalamus is thought to result in hyperkinesias like dystonia, and excess inhibition can result in hypokinesias such as Parkinson's[5, 7]. During normal behavior, however, premotor signals in primate thalamus are not easily explained by pallidal inputs alone[8, 9] and even persist following pallidal inactivation[10], leading to some question about the origins of activity in pallido-recipient thalamic areas[11-13].

Songbirds offer a tractable model system to study the origins of neural activity in motor thalamus. The vocal portion of the songbird BG-recipient thalamic nucleus DLM (dorsolateral division of the medial thalamus) is part of a premotor thalamocortical circuit essential for song learning (Fig. 1a–b)[14, 15]. Lesions to DLM or its target, the frontal cortical nucleus LMAN (lateral magnocellular nucleus of the anterior nidopallium), abolish vocal babbling and variability in juvenile birds[16, 17]. Because the pallidal projection to DLM terminates at a presynaptic terminal large enough to be recorded extracellularly (Fig. 1c), songbirds provide an opportunity to record simultaneously from a thalamic neuron and its presynaptic pallidal input[18-20].

Correspondence to: Michale S. Fee, fee@mit.edu.

Author contributions JHG and MSF designed the experiments and wrote the manuscript. JHG conducted the experiments.

To investigate the origins of thalamic activity during behavior, we have recorded from antidromically-identified thalamocortical neurons, as well as their pallidal and cortical inputs in singing juvenile birds. Premotor signals in DLM were not easily explained by pallidal inputs alone and persisted following pallidal lesion. Instead, our findings support the idea that descending cortical inputs drive song-locked rate modulations in BG-recipient thalamus[10, 12], and support a role for the thalamus in linking distinct cortical motor areas important for exploratory behavior during learning[21].

RESULTS

Thalamic neurons are activated during singing

To understand the role of the thalamus in song production, we recorded from neurons in the vocal portion of DLM in freely behaving juvenile zebra finches[22] (Fig. 1c–d, Supplementary Figs. 1–2, see Methods). Many of these neurons were antidromically-identified as thalamocortical neurons projecting to LMAN (n = 17/29, see Methods). The other 12 neurons did not respond to LMAN stimulation with a short-latency spike, but exhibited spike waveforms, firing patterns and correlations to song temporal structure similar to the identified projection neurons, and were included in the analysis. While DLM neurons recorded in anesthetized birds discharge at very low rates (< 10 Hz)[18-20], in awake birds they exhibited high average firing rates and were further activated during singing (Fig. 1d, singing: 89.0 ± 39.7 Hz vs. awake, non-singing: 60.7 ± 30.4 Hz, $P < 0.001$, paired t-test, n = 25/29, 11 birds, mean ± s.e.m. unless otherwise noted). Thalamic neurons also exhibited increased peak firing rates during singing (95th percentile rate: 394.4 ± 26.8 Hz vs. 196.9 ± 13.8 Hz, n = 29/29 neurons, $P < 0.001$ paired t-tests). These periods of high frequency firing (Fig. 1d–e) differed from low threshold bursts previously observed in mammalian thalamic neurons during low arousal states[23], and in DLM neurons in anesthetized birds[18-20]. Two common criteria for low threshold bursts are burst refractory periods (>50 ms) and a period of quiescence (>50 ms) prior to burst onset[24]. We did not observe thalamic discharge events that met these criteria. Instead, brief periods of high tonic discharge (HTD)—defined as firing events greater than 250 Hz (see Methods)—were generated from high background firing rates (>100 Hz) and did not exhibit refractory periods (Supplementary Fig. 1). HTD events were more common during singing compared to awake, non-singing periods (singing: 11.2 ± 1.3 HTDs s^{-1} vs. non-singing: 2.4 ± 0.8 HTDs s^{-1}, n = 28/29 neurons, $P < 0.001$, paired t-test, see Methods).

We examined the temporal relation between DLM activity and song vocalizations. In the youngest birds (< 45 days post hatch, dph), which generate subsong—highly random vocalizations akin to babbling—almost all DLM neurons were strongly activated at syllable onsets, exhibiting an average rate increase of 13.5 ± 1.9 Hz that began 27.1 ± 6.2 milliseconds prior to syllable onsets (Fig. 1e–f, $P < 0.05$ in 13/14 cells, see Methods). Prior to syllable offsets, most DLM neurons were briefly suppressed by an average of 8.2 ± 1.2 Hz ($P < 0.05$ in n = 11/14 cells), and this suppression began 40.0 ± 9.1 ms prior to syllable offsets (Fig. 1g). Given that DLM lesions abolish vocal babbling[17], these rate modulations could play a role in driving the initiation and termination of syllables in early song vocalizations.

After the subsong stage (>45 dph), juvenile birds begin singing ‘plastic’ song, which contains distinct, identifiable syllables of relatively fixed duration[25, 26]. All DLM neurons recorded at this stage exhibited song-locked rate modulations, but the timing of these modulations was much less homogeneous than in subsong birds. Specifically, in plastic song birds a given DLM neuron could exhibit rate peaks or dips at various times in syllable-aligned PSTHs, although there was a trend for neurons to exhibit peaks prior to syllable onsets (n = 7/15) and dips prior to syllable offsets (n = 7/15) (Supplementary Fig. 2).

Pallidal inputs to thalamus are activated during singing

We next set out to determine the origins of the remarkably homogenous syllable-locked signals observed in DLM of subsong birds. In both songbirds and mammals, thalamic rate increases can be facilitated by 'pauses' in the spiking of inhibitory pallidal inputs[4, 19]. Thus we hypothesized that pallidal inputs to DLM would exhibit average firing rate modulations opposite those of DLM neurons, i.e. rate suppression prior to syllable onsets and activation prior to syllable offsets. To test this hypothesis, we recorded, during singing, from the calyceal pallidal axon terminals that form 1:1 synaptic contacts with DLM neurons[18-20, 27] (Fig. 1c). We also recorded from the cell bodies (in the BG homologue Area X, see Fig 1a–b) of putative DLM-projecting pallidal neurons that give rise to the pallidal terminals in DLM (n = 17 cells, 4 birds, Supplementary Fig. 3)[18, 22]. Surprisingly, pallidal inputs also exhibited increased average firing rates during subsong (Fig. 1h, non-singing: 144.4 ± 27.8 Hz vs. singing: 296.0 ± 14.4, $P < 0.001$ paired tests, n = 14/14 terminals), as well as a peak in firing rate prior to subsong syllable onsets (Fig. 1j–k, rate increase of 17.1 ± 2.4 Hz, beginning 41.4 ± 2.6 ms prior to onsets, $P < 0.05$ in 12/14 terminals), and a decrease in firing rate prior to syllable offsets (Fig. 1m, rate decrease of 7.0 ± 2.3 Hz, beginning 51.4 ± 8.0 ms prior to offsets, $P < 0.05$ in 8/14 terminals). Contrary to what would be expected if thalamic signals were simply inverting pallidal inputs, no pallidal axon terminals recorded in DLM or pallidal cell bodies recorded in Area X (Supplementary Fig. 2) exhibited either an average firing rate decrease prior to subsong syllable onsets or a firing rate increase prior to subsong syllable offsets.

Coactivation of connected pallidal and thalamic neurons

These results raise several important questions. First, how do thalamic neurons discharge at high rates (~100 Hz) in the face of highly active pallidal inputs (~300 Hz)? One possibility is that the pallidal inputs are not as strongly inhibitory as previously believed[27]. To test this possibility, we recorded simultaneously from LMAN-projecting DLM neurons, together with the putative presynaptic axon terminal, at the end of the same electrode[18-20] in awake behaving birds (Fig. 2a–c, Supplementary Figs. 4–6, n = 7 pairs total, 5 pairs in juvenile birds, 4 of which were recorded during singing, and an additional 2 pairs in singing adults, see Methods). In all pairs, the pallidothalamic interaction was indeed strongly inhibitory; thus results from both adults and juveniles were pooled in the following analysis (Supplementary Fig. 5). Rasters of thalamic spikes, aligned to simultaneously-recorded pallidal spikes, revealed that each pallidal spike was followed by a period of absolute thalamic spike suppression (Fig. 2d–e), similar to what is observed in pairs recorded in anesthetized birds[18-20]. However, the duration of this suppression, measured as the latency from each pallidal spike to the following thalamic spike, was extremely brief during singing (5.2 ± 0.6 ms, n = 6 pairs), significantly shorter than previously observed under anesthesia (~20 ms)[18-20]. Following this suppression, thalamic neurons spiked with a high probability in a narrow time window, resulting in a large, narrow peak in the pallido-thalamic cross correlogram (Fig. 2f, Supplementary Fig. 5). During signing, the standard deviation of this peak was extremely small (0.82 ± 0.2 ms, n = 6 pairs), indicating that the first thalamic spike that occurred in a pallidal interspike interval was locked to the preceding pallidal spike with submillisecond precision.

While pallidal inputs were strongly inhibitory, thalamic spiking was not restricted to pallidal 'pauses'. The duration of DLM spike suppression (5%–95% range: 3.9 ± 0.5 – 6.9 ± 0.9 ms, n = 6 pairs) was well within the distribution of the simultaneously-recorded pallidal interspike intervals (Fig. 2e–g, Supplementary Fig. 5, mean: 4.0 ± 0.5 ms, 5%-95% range: 2.2 ± 0.2 – 7.2 ± 1.1 ms, n = 6 pairs). Across all pairs, one or more thalamic spikes occurred in 23.1 ± 8.8% of pallidal ISIs during singing. Notably, thalamic neurons spiked sooner after the preceding pallidal spike during singing than during non-singing periods (non-singing:

8.0 ± 0.7 ms vs. singing: 5.2 ± 0.6 ms, $P < 0.001$ in 6/6 pairs), enabling thalamic neurons to discharge at rates in excess of ~100 Hz during singing even in the presence of powerfully inhibitory inputs occurring at ~300 Hz (Fig. 2f,p). In summary, thalamic neurons were able to discharge at high rates during singing because each pulse of pallidal inhibition was so brief.

We wondered if this brief, millisecond-timescale inhibition exerted by pallidal inputs had a net suppressive effect on thalamic firing rates on broader timescales, or whether it might instead effectively increase thalamic firing rates, for example by the post-inhibitory rebound mechanism observed under anesthesia[18]. Pallidal suppression of thalamic firing rate was visibly apparent in the simultaneously recorded spike trains (Fig. 2g, Supplementary Fig. 5d). The suppression of thalamic spikes by pallidal spikes was quantified with a standard spike train cross-correlation analysis in large (10 ms) time bins (Supplementary Fig. 6g), as well as the cross-correlation between pallidal and thalamic instantaneous firing rates (IFRs) during singing (Fig. 2h–j) (median width at half-minimum: 19.4 ± 10.6 ms; zero lag cc: −0.44 ± 0.04, $P < 0.01$, n = 6/6 pairs, see Methods). Both of these analyses confirmed that pallidal and thalamic firing rates were significantly anti-correlated, and that, on average, pallidal rate increases were associated with thalamic rate decreases, and vice versa.

We wondered if pallidal inputs were also inhibitory at syllable onsets and offsets. In the paired recordings, we plotted the number of pallidal spikes that occurred in the 30 milliseconds prior to each syllable onset against the number of thalamic spikes that occurred in the same period, and found that they were strongly anti-correlated in all pairs. Rate changes prior to syllable offsets were also anti-correlated (Fig. 2k–m, Onsets: −0.61 ± 0.04, Offsets: −0.62 ± 0.07, $P < 0.001$, n = 6/6 pairs). Together, these findings demonstrate that increases in pallidal firing rate were associated with a suppression of thalamic spiking, even at syllable onsets and offsets.

Pallidal suppression of thalamic spiking was also evident within single pallidal ISIs. The number of thalamic spikes that discharged within a single pallidal ISI was strongly linearly dependent on duration of that ISI (r = 0.80 ± 0.05, n = 6 pairs during singing), i.e. longer pallidal ISIs contained more thalamic spikes, consistent with previous observations in anesthetized birds (Fig. 2n)[19]. During singing, the first thalamic spike occurred on average 5.2 ± 0.6 ms after a pallidal spike, and an additional thalamic spike discharged for every 3.9 ± 0.6 ms increase in the duration of the pallidal ISI (data are mean ± S.E.M. for 6 pairs during singing). We used this empirical relation between pallidal ISI and thalamic spiking to predict thalamic spiking in response to each pallidal spike train recorded during subsong (Supplementary Fig. 8). Consistent with the result that pallidal inputs suppressed thalamic spiking (Fig. 2g–n), simulated thalamic activity exhibited rate decreases prior to syllable onsets, and rate increases prior to offsets (Supplementary Fig. 8), exactly the opposite of what was actually observed. Together, these findings suggested that pallidal inputs were not driving the thalamic rate changes observed at subsong syllable onsets and offsets (Fig. 1g–h).

Activation of thalamic neurons in Area X lesioned birds

We hypothesized that thalamic firing patterns might be driven by non-pallidal inputs. If this is true, then DLM neurons should exhibit these modulations even after removal of pallidal inputs. To test this possibility, we recorded LMAN-projecting DLM neurons in Area X-lesioned birds (Fig. 3a–b, n = 3 birds, see Methods). As in intact birds, DLM neurons in lesioned birds were more active during singing than non-singing, exhibiting higher average firing rates (Fig. 3c, non-singing: 25.6 ± 14.7 Hz vs. singing: 58.6 ± 23.6 Hz, $P < 0.05$ paired t-test, n = 6/6 neurons). DLM neurons in Area X-lesioned birds also exhibited the same song-locked rate modulations observed in intact birds (Fig. 3d–f). They showed

increased firing rate at syllable onsets (average 20.0 ± 5.1 Hz increase starting 40.0 ± 6.8 milliseconds prior to onsets, $P < 0.05$ in 6/6 cells) and decreased firing rate prior to syllable offsets (average 13.0 ± 2.6 Hz decrease starting 26.0 ± 12.1 ms prior to offsets, $P < 0.05$, 5/6 cells). Thus, song-locked rate modulations in DLM did not require pallidal inputs, suggesting the involvement of other inputs to the thalamus.

A corticothalamic projection drives thalamic spiking *in vivo*

What, then, gives rise to the three aspects of subsong-related firing rate modulations observed in thalamic neurons: 1) overall activation during singing, 2) rate increases prior to syllable onsets and 3) rate decreases prior to syllable offsets? To identify non-pallidal inputs to DLM, we injected retrograde tracer into DLM and observed labeling of a subpopulation of neurons in the motor cortical nucleus RA (robust nucleus of the arcopallium, Fig. 4a–d, n = 3 birds, see Methods), consistent with previous reports[28, 29]. Furthermore, injections of a virus expressing green fluorescent protein (GFP) into RA revealed extensive axonal terminations in the LMAN-projecting part of DLM (n = 3/3 birds, Fig. 4e–h, Supplementary Fig. 11). This presumably glutamatergic projection[28] is analogous to corticothalamic pathways found in mammals (Fig. 1b)[6, 21].

To test if the descending projection from RA could drive spiking in DLM, we recorded DLM neurons in anesthetized juvenile birds during electrical stimulation of RA (see Methods). Because stimulation in RA could potentially influence DLM through Area X (by antidromic activation of HVC and LMAN), Area X was inactivated during these experiments (Fig. 5a, Supplementary Figs. 9–10, see Methods,). RA stimulation strongly activated DLM neurons, causing a significant increase in firing rate (Supplementary Fig. 9, Fig. 5b–d, average rate increase = 106.0 ± 17.3 Hz, $P < 0.01$ in 37/39 neurons, n = 9 birds, see Methods) at low latencies (Fig. 5e,f, 12.6 ± 0.8 ms, n = 37 neurons). These findings demonstrated the functionality and excitatory nature of the corticothalamic projection from RA to DLM.

Cortical inputs to thalamus are activated during singing

To further examine the idea that syllable-related thalamic rate modulations are driven by these cortical inputs, we recorded antidromically-identified neurons in RA that project to DLM (RA_{DLM} neurons) in singing juvenile birds (Fig. 6a–d). Of 115 neurons recorded in RA of five subsong birds, 17 were antidromically-identified as projecting to DLM. RA_{DLM} neurons exhibited remarkably homogenous firing patterns. All neurons showed increased average firing rates during singing (non-singing: 18.2 ± 2.2 Hz vs. singing: 44.2 ± 7.7, $P < 0.001$ paired t-test). All neurons also showed a peak in firing rate prior to syllable onsets (Fig. 6e–f, rate increase of 21.0 ± 4.8 Hz, $P < 0.05$ in 17/17 cells), and most neurons exhibited a decrease in firing rate prior to syllable offsets (Fig. 6g, rate decrease of 13.0 ± 4.4 Hz, $P < 0.05$ in 15/17 cells). In contrast, neurons not identified as DLM-projectors exhibited a range of different firing patterns (Supplementary Fig. 12). Notably, the rate increase at syllable onsets occurred significantly earlier in RA_{DLM} neurons than in DLM neurons (Fig. 6h, RA_{DLM}: 43.7 ± 4.5 ms vs. DLM: 27.1 ± 6.2 ms, $P < 0.05$, t-test) and trended to earlier times for the rate decrease prior to syllable offsets (RA_{DLM}: 48.2 ± 6.2 ms vs. DLM: 40.0 ± 9.1 ms, $p>0.2$). Thus, both the amplitude and the timing of rate modulations in RA_{DLM} neurons were consistent with a role in driving thalamic activity during singing. Of course we cannot rule out the additional possible involvement of other, uncharacterized, inputs to DLM.

Examining the pallidal, thalamic and corticothalamic firing patterns side-by-side revealed that the excitatory cortical inputs to the thalamus were temporally matched by the inhibitory pallidal inputs at syllable onsets and offsets, as well as during the transitions into and out of

singing (Fig. 6h–j). While the timing of inhibitory and excitatory inputs was closely balanced, the relative magnitudes of the rate modulations, when normalized by the baseline firing rate, were significantly larger in RA_{DLM} neurons than in both the pallidal inputs and the DLM neurons themselves ($P < 0.01$ in t-tests for all comparisons, see Methods). These large fractional changes in firing rate of the RA_{DLM} neurons may explain how they were able to drive thalamic activity in the face of opposing inhibitory signals during singing.

DISCUSSION

We examined the origins of neural activity in DLM, a BG-recipient thalamic nucleus necessary for vocal babbling in juvenile birds[17]. DLM neurons were strongly activated during singing and exhibited peaks in firing rate immediately prior to subsong syllable onsets. Paradoxically, pallidal inputs to DLM, although inhibitory, were also activated during singing and prior to syllable onsets. We hypothesized a role for non-pallidal inputs to DLM, and found that song-locked thalamic rate modulations persisted following lesion of pallidal inputs and that activation of cortical inputs to DLM from the motor nucleus RA drove DLM neurons *in vivo*. Consistent with a role in driving DLM signals during behavior, antidromically-identified corticothalamic neurons were activated during singing and exhibited rate peaks prior to syllable onsets. Together, these findings suggest that cortical inputs can be the principle drivers of behavior-locked activity in the BG-recipient motor thalamus[12].

Do our findings apply to mammalian BG-thalamocortical circuits? In mammals, the role of pallidal inhibition in controlling thalamic activation and the initiation of movement is widely recognized[3-5]. However, thalamic signals are not easily explained by pallidal inputs alone during behavior[8, 9, 12]. For example, in cued saccade or arm movement tasks in primates, most thalamic neurons exhibit a brisk peak in activity immediately prior to movement onset[8, 9, 13], similar to the rate peak observed prior to syllable onsets in the present study. In contrast to what would be predicted if these signals were driven by pauses in pallidal activity[4], most pallidal neurons in these tasks also exhibit rate increases at movement onset[13, 30-34], similar to the pallidal terminals observed in the present study.

At least two explanations have been put forward to reconcile observed ‘paradoxical’ pallido-thalamic co-activations observed during behavior. First, thalamic spiking can be driven directly by pallidal rate increases through a post-inhibitory rebound mechanism. In this model, increased pallidal activity hyperpolarizes thalamic neurons, causing de-inactivation of low threshold calcium channels. Following a brief pallidal pause, these calcium channels then trigger a ‘rebound’ thalamic burst[23, 35]. Rebound spiking is observed in DLM neurons in brain slice and in anesthetized songbirds[18, 20, 36], where both pallidal axon terminals and connected thalamic neurons are co-activated during song playback or cortical stimulation[18, 20].

The rebound model does not easily fit with our results during singing. First, the calcium channels that drive rebound spikes rapidly inactivate at depolarized membrane potentials[37]. Thus, rebound spiking is associated with low levels of thalamic activation, such as during drowsiness, anesthesia or sleep[23]. Indeed, DLM neurons discharge at very low rates in anesthetized birds (<10 Hz)[18-20], more than an order of magnitude lower than we observed during singing (~100 Hz). Second, rebound bursts trigger calcium channel inactivation[23] and are followed by a substantial (>50 ms) burst refractory periods in DLM neurons *in vitro*[36]. We found that DLM neurons generated high tonic discharge events (>250 Hz) from high baseline firing rates (~100 Hz), and these events did not exhibit refractory periods (Supplementary Fig. 1). Finally, DLM neurons exhibited song-locked rate modulations following lesion of pallidal inputs (Fig. 3). Thus, while our results do not rule out a possible

role for low threshold calcium channels, they do indicate that song-locked signals in DLM do not require inhibitory pallidal inputs, and therefore do not require a post-inhibitory rebound mechanism.

A second possible explanation for 'paradoxical coactivations' observed in pallidal and thalamic neurons arises from the fact that pallidal and thalamic neurons were previously only recorded separately during behavior. Thus, it was not known if activated pallidal and thalamic neurons were in fact synaptically connected, or rather were recorded from different 'channels' of the BG-thalamic circuit[38]. In this view, pallidal neurons that exhibit rate increases at movement onset could effectively suppress some thalamic neurons, while at the same time pallidal neurons in a different channel could exhibit rate decreases that, through disinhibition, activate other thalamic neurons[3, 38, 39]. In the absence of information about the synaptic connectivity of these neurons, the activated pallidal and activated thalamic neurons might be interpreted as showing paradoxical coactivation, when in fact there is no actual coactivation within a single BG-thalamic channel.

By recording from connected pallidal and thalamic neurons during vocal babbling, we showed that pallidal and thalamic coactivations can occur in the same BG-thalamic 'channel.' Our data suggest that this occurs because thalamic activity is driven by excitatory cortical inputs that oppose the temporally matched inhibitory inputs from the BG. This tendency of pallidal and $RA_{(DLM)}$ neurons to exhibit similar firing patterns during singing could result form their common inputs from HVC, a hypothesis that could be tested by recording from Area X, DLM and RA in HVC-lesioned birds. Notably, similar excitation-inhibition matching is observed in cortex and is suggested to play a role in temporal gating of sensory inputs[40, 41].

While our data suggest a key role for cortical inputs to thalamus, we also found that BG outputs have a substantial impact on thalamic activity. Consistent with the inhibitory nature of the pallidothalamic synapse[4, 10, 13, 18-20, 27], the activities of synaptically connected pallidal and DLM neurons were strongly anti-correlated during singing: pallidal rate increases were associated with thalamic rate decreases, and vice versa, even at syllable onsets (Fig. 2g–m, Supplementary Fig. 8). In addition, consistent with a role of pallidal inputs in controlling thalamic spike timing[20, 36], DLM spikes were entrained to preceding pallidal spikes with submillisecond precision (Fig. 2d–f). These findings clearly demonstrate that pallidal inputs are important modulators of thalamic activity during behavior. However, pallidal modulation of thalamic activity does not appear necessary for aspects of thalamic motor function, as thalamic premotor signals persisted following lesion of BG inputs (Fig. 3), and BG lesions in juvenile and adult birds have little, if any, immediate effect on song structure[15, 17].

What, then, are the functions of the songbird BG? Area X lesions result in protracted song variability and poor imitation[15], but the reasons for this remain unclear. We suggest two possible explanations. First, LMAN driven variability is biased in such a ay to reduce vocal errors[43, 44], and the song-locked pallidal rate modulations observed here and in a previous study[22] may play a role in biasing variability to drive learning[45]. Second, pallidal control of thalamic spike timing could play a role in regulating spike-timing dependent plasticity to direct learning in downstream motor cortical circuits[46, 47].

In summary, while pallidal inputs clearly produce large modulations in thalamic firing rates, here we show that cortical inputs may act as principle drivers of behavior-locked activity in the thalamus[12]. We have also recently found that vocal babbling requires two cortical areas (RA and LMAN) as well as the BG-recipient thalamus (DLM) that interconnects them, but not the BG itself[16, 17]. Our results support the idea that the BG-recipient thalamus mediates

interactions between cortical areas important for behavior[21]. For example, RA, DLM and LMAN could form a reverberant cortico-thalamocortical loop that generates vocal babbling. In addition, corticothalamic signals may play a role in driving learning in cortical circuits. In particular, signals transmitted from RA to DLM could be involved in the early development of stereotyped vocal structure in the songbird[25, 26], or in the biasing of motor output towards improved behavioral performance during learning[43-45]. Because songbird cortical areas differ from mammalian cortex in several ways[48, 49] it will be necessary to test if corticothalamic projections in mammals play a similar role in driving BG-recipient thalamus during exploratory behavior and learning.

METHODS

Animals

Subjects were juvenile male zebra finches (n = 26) at the subsong stage of song development (36–55 dph), and one additional young adult (110 dph) singing undirected song. Excitotoxic lesions to Area X were performed in an additional 3 birds (50–60 dph) as described below. Birds were obtained from the Massachusetts Institute of Technology zebra finch breeding facility (Cambridge, Massachusetts). The care and experimental manipulation of the animals were carried out in accordance with guidelines of the National Institutes of Health and were reviewed and approved by the Massachusetts Institute of Technology Committee on Animal Care.

Chronic neural recordings and histology

Using motorized microdrives for chronic neural recordings, electrodes were implanted into DLM (n = 11 birds), RA (n = 5 birds) or Area X (n = 4 birds), and recordings were carried out as described previously[22]. Units accepted for analysis had signal-to-noise ratios (average spike peak amplitude compared with s.d. of noise) of >10:1. Antidromic identification of LMAN-projecting DLM neurons, and DLM-projecting RA neurons, was carried out with a bipolar stimulating electrode implanted in LMAN or DLM using techniques described previously (stimulation intensities: 50–300 μA for 200 μs). All of the antidromically-identified DLM and RA neurons in our dataset were further validated with collision tests. At the conclusion of experiments, small electrolytic lesions (20 μA for 15 s) were made through the recording and stimulation electrodes for histological verification of electrode positions. Of the 29 DLM neurons, 17 were antidromically-identified and collision tested. The other 12 neurons did not respond to LMAN stimulation with a short-latency spike, but exhibited spike waveforms, firing patterns and correlations to song temporal structure similar to the identified projection neurons, and were included in the analysis. We suspect that these were LMAN-projecting DLM neurons, but that they did not project to the part of LMAN activated by the stimulation electrode in DLM. Of 115 neurons recorded in RA, 17 were antidromically-identified and collision tested as DLM-projecting.

RA neurons terminate in both DLM and the nearby dorsomedial thalamic nucleus (DMP), just posterior and medial to DLM[50] (see Fig. 4e–h and Supplementary Fig. 11). This raises the possibility that our antidromic stimulating electrode in DLM may activate not just fibers that terminate in DLM, but also those that terminate in DMP. We have observed single RA axons branching and coursing through both DLM and DMP (Supplementary Figure 10), suggesting that some individual RA neurons may project to both DLM and DMP. However, if there are neurons that project only to DMP, we cannot rule out the possibility that our antidromic stimulation procedure might identify neurons projecting only to DMP. However, given the remarkable homogeneity of firing patterns of thalamus projecting RA neurons, it seems likely that our conclusions about the nature of the signal being transmitted to DLM would be altered by this fact. As a separate issue, it is also possible that some of the neurons

that were not antidromically-identified may also have been DLM-projectors, but these were analyzed separately (Supplementary Fig. 12).

To visualize pallidal terminals and thalamic neurons in DLM (as in Fig. 1c), Alexa Dextran-555 (Molecular probes) was injected into Area X, for anterograde labeling of calyceal terminals, and Alexa dextran-647 into LMAN for retrograde labeling of DLM neurons. For DLM tract-tracing experiments (Fig. 4), Alexa Dextran-555, or Cholera toxin beta subunit (Molecular probes) was injected into DLM, MMAN or LMAN. For anterograde tracing of RA axons terminating in DLM and DMP, herpes virus expressing GFP on a CMV promoter, obtained from the MIT viral core facility, was injected into RA. 100μm brain slices were imaged with a Nikon PCM2000 confocal microscope, and ImageJ was used to merge serial sections. All histological figures show sagittal sections.

Targeting DLM—We targeted the Area X-recipient portion of DLM for recording as follows. Prior to microdrive implantation, the antero-posterior and dorso-ventral extent of this region was determined by electrophysiologically mapping the high frequency firing, thin-spiking pallidal axon terminals that constitute Area X outputs[18, 22]. We have found that the medial zone of the pallidal terminal region does not exhibit singing-related firing patterns. This region likely corresponded to the ventromedial portion of DLM that is not innervated by Area X and that projects to a shell surrounding LMAN[50]. We have found that the center of the singing-related Area X-recipient zone is reliably located at 1.07 mm lateral to the midline. Thus, using a head angle of 65 degrees relative to the flat anterior portion of the skull, electrodes were targeted to the center of Area X recipient portion of DLM: 1.07 mm lateral to midline, and, depending on the individual bird, between +0.9 to 1.5 mm anterior to the bifurcation of the mid-sagittal sinus (lambda), and ~4.3 mm ventral to the brain surface. Using this technique, we reliably recorded from LMAN projecting DLM neurons, and avoided DMP, a nearby thalamic nucleus where pallidal axon terminals are not observed in extracellular recordings (Supplementary Fig. 10).

Area X lesion methods and histological confirmation—Bilateral excitoxic lesions of Area X were made by injecting 200 nL of 4% N-Methyl-DL aspartic acid (NMA, Sigma) into the center of each Area X (head angle 20 degrees, 5.8 mm anterior, 1.5 mm lateral, and 2.85 mm ventral), and an additional 50 nL into each medial Area X, using stereotactic coordinates (head angle 20 degrees, 5.8 anterior, 1.2 mm lateral, 2.6 mm ventral). Recording and stimulating electrodes were implanted into DLM and LMAN, respectively, immediately following the Area X lesion (during the same surgery). Birds rapidly recovered from the lesion and began singing within 2–4 days. In the present study, recordings were acquired from singing birds between 5–12 days following the Area X lesion. In a previous study, this lesion protocol reliably lesions between 80–100% of Area X (n = 19 birds)[17]. As described previously, lesions were confirmed histochemically using fluorescent antibody to neuronal nuclei (Mouse anti- Neu-N, Millipore); Area X stained brighter than background in Neu-N staining and lesion boundaries were clearly visible[17]. In addition to histological confirmation, Area X lesions were functionally confirmed: whereas pallidal terminals are always observed in electrode penetrations through DLM of control birds, terminals were never observed in DLM of Area X lesioned birds.

Statistical analysis

We represented neural activities as instantaneous firing rates, R(t), defined at each time point as the inverse of the enclosing interspike interval as follows:

$$R(t)=\frac{1}{t_{i+1}-t_i},\ \text{for}\ t_i<t\leq t_{i+1}$$

where t_i is the time of the i^{th} spike. Note that IFRs are computed as the inverse of the interspike interval for the duration of that interval, and thus they measure firing rate. Thus, the IFR cross correlation analysis (as in Fig. 2h) computes the relation between pallidal and thalamic firing rates. In contrast, a standard cross correlogram analysis (as in Fig. 2f) computes the spiking probability in a temporally defined bin.

Spike sorting and analysis—Spikes were sorted offline using custom Matlab software (Aaron Andalman, Dmitry Aronov, JG and MSF). DLM spikes were distinguished from pallidal terminals by their wider spike widths, lower mean firing rate during non-singing periods, and by antidromic activation from LMAN, as previously described[22]. To sort spikes from pairs simultaneously recorded on the same electrode, we developed a template-matching spike sorting algorithm that automatically detected and assigned identity to spike overlaps. See Supplementary Fig. 4 for a detailed description of the spike sorting procedure. High tonic discharge (HTD) events[9] in DLM were defined as firing events exceeding 250 Hz. We tested different thresholds between 200 and 300 Hz, and in all cases HTDs were generated from high levels of background activity. They were more frequent during singing and did not exhibit refractory periods (Supplementary Fig. 1).

Analysis of correlations of neural activity to song temporal structure—Neural activity was aligned to the 300 ms preceding and following all syllable onsets and offsets. Only cells recorded for greater than 50 syllables were accepted. To determine the significance of firing rate peaks and troughs, a rate histogram (bin size, 10 ms) was generated of the real data (as in Fig. 1f). Then a surrogate histogram was generated in which each trial of syllable-aligned neural activity was time-shifted by a uniformly distributed random amount over a range equal to the duration of the histogram (600 ms). The shift was circular, such that spikes wrapped around to the beginning of the histogram, preserving the overall spike statistics of the data. The minimum and maximum of the surrogate rate histogram was then obtained with 1000 repetitions of randomly shifted data. *P*-values for the rate minima and maxima of the real data set were calculated by analyzing the frequency with which shifted data sets generated larger maxima or smaller minima in firing rates. Peaks and troughs in firing rate with *P*-values <0.05 were considered significant.

The amplitude of the rate modulation was computed as the maximal deviation from the rate from a baseline period of the histogram (−300 to −200 ms prior to syllable onset or offset). The timing of the rate change relative to the syllable onset (or offset) was computed as the time at which the rate change surpassed two standard deviations above (for rate increases) or below (for rate decreases) the baseline rate. Using different criteria for the detection of the rate change, including 1, 3 and 4 standard deviations from the mean, did not significantly alter our conclusions.

To construct population rate histograms (as in Fig. 1g, bottom) data from individual cells were mean-subtracted and then averaged across the group. To compute fractional changes in firing rates at the onsets and offsets of syllables and singing epochs (as in Fig. 6h–j), we normalized the mean-subtracted rate histogram by the mean rate in the baseline period. Lag cross-correlations for the paired pallidothalamic recordings were computed using the xcorr function in Matlab. The significance of the anti-correlation at zero time lag was computed using the corrcoef function.

Assessing the functionality of the RA projection to DLM

In subsong-aged anesthetized birds (n = 9 birds, 35–49 dph), a bipolar stimulation electrode was implanted in RA, and a custom-fabricated reverse microdialysis probe[16] (Supplementary Fig. 9) was implanted in Area X. Recording electrodes were targeted to the Area X-recipient portion of DLM, as described[18, 22]. Pallidal terminals were recorded as muscimol (1.5 mg mL^{-1}) or tetrodotoxin (1μM) (Sigma-Aldrich) was infused through the dialysis probes. Inactivation of Area X was confirmed by the disappearance of pallidal activity (Supplementary Fig. 7f), as described[19]. DLM neurons were recorded during either burst-stimulation in RA (each burst consisted of 3–5 stimulations at 500 Hz, 200μs pulse width, 60–150 μA stimulus current, bursts delivered at 0.5 or 1 Hz), or during single-stimulation in RA (single stimulations delivered at 0.5 or 1 Hz, 60–150 μA stimulus current, Supplementary Fig. 9). The latency of the DLM response to RA stimulation was computed as the time in the PSTH (binsize 5 ms) where the rate exceeded 2 S.D. above baseline period of 0.3 seconds prior to the stimulation. To assess the significance of the rate change following RA stimulation, rate histograms were subjected to the same statistical analysis described above for syllable onsets.

Supplementary Material

Refer to Web version on PubMed Central for supplementary material.

Acknowledgments

We thank Ann Graybiel and Michael Farries for comments on the manuscript. Funding to MSF was provided by the NIH (grant # R01DC009183) and to JHG by the NIH (grant # K99NS067062), and the Charles King Trust and Damon Runyon Research Foundation post-doctoral fellowships.

References

1. Graybiel AM. The basal ganglia: learning new tricks and loving it. Curr Opin Neurobiol. 2005; 15:638–644. [PubMed: 16271465]
2. Reiner, A. The Basal Ganglia IX. Springer; New York: 2009. You cannot have a vertebrate brain without a basal ganglia; p. 3-24.
3. Hikosaka O. GABAergic output of the basal ganglia. Prog Brain Res. 2007; 160:209–226. [PubMed: 17499116]
4. Chevalier G, Deniau JM. Disinhibition as a basic process in the expression of striatal functions. Trends Neurosci. 1990; 13:277–280. [PubMed: 1695403]
5. DeLong MR. Primate models of movement disorders of basal ganglia origin. Trends Neurosci. 1990; 13:281–285. [PubMed: 1695404]
6. Kultas-Ilinsky K, Sivan-Loukianova E, Ilinsky IA. Reevaluation of the primary motor cortex connections with the thalamus in primates. J Comp Neurol. 2003; 457:133–158. [PubMed: 12541315]
7. Albin RL, Young AB, Penney JB. The functional anatomy of basal ganglia disorders. Trends Neurosci. 1989; 12:366–375. [PubMed: 2479133]
8. Strick PL. Activity of ventrolateral thalamic neurons during arm movement. J Neurophysiol. 1976; 39:1032–1044. [PubMed: 824408]
9. Anderson ME, Turner RS. Activity of neurons in cerebellar-receiving and pallidal-receiving areas of the thalamus of the behaving monkey. J Neurophysiol. 1991; 66:879–893. [PubMed: 1753292]
10. Inase M, Buford JA, Anderson ME. Changes in the control of arm position, movement, and thalamic discharge during local inactivation in the globus pallidus of the monkey. J Neurophysiol. 1996; 75:1087–1104. [PubMed: 8867120]
11. Deniau JM, Lackner D, Feger J. Effect of substantia nigra stimulation on identified neurons in the VL-VA thalamic complex: comparison between intact and chronically decorticated cats. Brain Res. 1978; 145:27–35. [PubMed: 638780]

12. Sherman, SM.; Guillery, RW. Exploring the Thalamus and Its Role In Cortical Function. MIT Press; Cambridge, MA: 2006.
13. Kunimatsu J, Tanaka M. Roles of the primate motor thalamus in the generation of antisaccades. J Neurosci. 2010; 30:5108–5117. [PubMed: 20371831]
14. Bottjer SW, Miesner EA, Arnold AP. Forebrain lesions disrupt development but not maintenance of song in passerine birds. Science. 1984; 224:901–903. [PubMed: 6719123]
15. Scharff C, Nottebohm F. A comparative study of the behavioral deficits following lesions of various parts of the zebra finch song system: implications for vocal learning. J Neurosci. 1991; 11:2896–2913. [PubMed: 1880555]
16. Aronov D, Andalman AS, Fee MS. A specialized forebrain circuit for vocal babbling in the juvenile songbird. Science. 2008; 320:630–634. [PubMed: 18451295]
17. Goldberg JH, Fee MS. Vocal babbling in songbirds requires the basal ganglia-recipient motor thalamus but not the basal ganglia. J Neurophysiol. 2011
18. Person AL, Perkel DJ. Pallidal neuron activity increases during sensory relay through thalamus in a songbird circuit essential for learning. J Neurosci. 2007; 27:8687–8698. [PubMed: 17687046]
19. Kojima S, Doupe AJ. Activity propagation in an avian basal ganglia-thalamocortical circuit essential for vocal learning. J Neurosci. 2009; 29:4782–4793. [PubMed: 19369547]
20. Leblois A, Bodor AL, Person AL, Perkel DJ. Millisecond timescale disinhibition mediates fast information transmission through an avian basal ganglia loop. J Neurosci. 2009; 29:15420–15433. [PubMed: 20007467]
21. McFarland NR, Haber SN. Thalamic relay nuclei of the basal ganglia form both reciprocal and nonreciprocal cortical connections, linking multiple frontal cortical areas. J Neurosci. 2002; 22:8117–8132. [PubMed: 12223566]
22. Goldberg JH, Adler A, Bergman H, Fee MS. Singing-related neural activity distinguishes two putative pallidal cell types in the songbird basal ganglia: comparison to the primate internal and external pallidal segments. J Neurosci. 2010; 30:7088–7098. [PubMed: 20484651]
23. Llinas RR, Steriade M. Bursting of thalamic neurons and states of vigilance. J Neurophysiol. 2006; 95:3297–3308. [PubMed: 16554502]
24. Jeanmonod D, Magnin M, Morel A. Low-threshold calcium spike bursts in the human thalamus. Common physiopathology for sensory, motor and limbic positive symptoms. Brain. 1996; 119(Pt 2):363–375. [PubMed: 8800933]
25. Veit L, Aronov D, Fee MS. Learning to breathe and sing: development of respiratory-vocal coordination in young songbirds. J Neurophysiol. 2011; 106:1747–1765. [PubMed: 21697438]
26. Aronov D, Veit L, Goldberg JH, Fee MS. Two distinct modes of forebrain circuit dynamics underlie temporal patterning in the vocalizations of young songbirds. J Neurosci. 2011; 31:16353–16368. [PubMed: 22072687]
27. Luo M, Perkel DJ. A GABAergic, strongly inhibitory projection to a thalamic nucleus in the zebra finch song system. J Neurosci. 1999; 19:6700–6711. [PubMed: 10414999]
28. Wild JM. Descending projections of the songbird nucleus robustus archistriatalis. J Comp Neurol. 1993; 338:225–241. [PubMed: 8308169]
29. Vates GE, Vicario DS, Nottebohm F. Reafferent thalamo- “cortical” loops in the song system of oscine songbirds. J Comp Neurol. 1997; 380:275–290. [PubMed: 9100137]
30. Georgopoulos AP, DeLong MR, Crutcher MD. Relations between parameters of step-tracking movements and single cell discharge in the globus pallidus and subthalamic nucleus of the behaving monkey. J Neurosci. 1983; 3:1586–1598. [PubMed: 6875658]
31. Anderson ME, Horak FB. Influence of the globus pallidus on arm movements in monkeys. III. Timing of movement-related information. J Neurophysiol. 1985; 54:433–448. [PubMed: 4031996]
32. Anderson ME, Turner RS. A quantitative analysis of pallidal discharge during targeted reaching movement in the monkey. Exp Brain Res. 1991; 86:623–632. [PubMed: 1761096]
33. Yoshida A, Tanaka M. Enhanced modulation of neuronal activity during antisaccades in the primate globus pallidus. Cereb Cortex. 2009; 19:206–217. [PubMed: 18477689]
34. Sheth SA, Abuelem T, Gale JT, Eskandar EN. Basal ganglia neurons dynamically facilitate exploration during associative learning. J Neurosci. 2011; 31:4878–4885. [PubMed: 21451026]

35. Pare D, Curro'Dossi R, Steriade M. Neuronal basis of the parkinsonian resting tremor: a hypothesis and its implications for treatment. Neuroscience. 1990; 35:217–226. [PubMed: 2199839]
36. Person AL, Perkel DJ. Unitary IPSPs drive precise thalamic spiking in a circuit required for learning. Neuron. 2005; 46:129–140. [PubMed: 15820699]
37. Coulter DA, Huguenard JR, Prince DA. Calcium currents in rat thalamocortical relay neurones: kinetic properties of the transient, low-threshold current. J Physiol. 1989; 414:587–604. [PubMed: 2607443]
38. Mink JW. The basal ganglia: focused selection and inhibition of competing motor programs. Prog Neurobiol. 1996; 50:381–425. [PubMed: 9004351]
39. Deniau JM, Chevalier G. Disinhibition as a basic process in the expression of striatal functions. II. The striato-nigral influence on thalamocortical cells of the ventromedial thalamic nucleus. Brain Res. 1985; 334:227–233. [PubMed: 3995318]
40. Okun M, Lampl I. Instantaneous correlation of excitation and inhibition during ongoing and sensory-evoked activities. Nat Neurosci. 2008; 11:535–537. [PubMed: 18376400]
41. Vogels TP, Abbott LF. Gating multiple signals through detailed balance of excitation and inhibition in spiking networks. Nat Neurosci. 2009; 12:483–491. [PubMed: 19305402]
42. Doupe AJ, Perkel DJ, Reiner A, Stern EA. Birdbrains could teach basal ganglia research a new song. Trends Neurosci. 2005; 28:353–363. [PubMed: 15935486]
43. Andalman AS, Fee MS. A basal ganglia-forebrain circuit in the songbird biases motor output to avoid vocal errors. Proc Natl Acad Sci U S A. 2009; 106:12518–12523. [PubMed: 19597157]
44. Warren TL, Tumer EC, Charlesworth JD, Brainard MS. Mechanisms and time course of vocal learning and consolidation in the adult songbird. J Neurophysiol. 2011; 106:1806–1821. [PubMed: 21734110]
45. Fee MS, Goldberg JH. A hypothesis for basal ganglia-dependent reinforcement learning in the songbird. Neuroscience. 2011; 198:152–170. [PubMed: 22015923]
46. Markram H, Lubke J, Frotscher M, Sakmann B. Regulation of synaptic efficacy by coincidence of postsynaptic APs and EPSPs. Science. 1997; 275:213–215. [PubMed: 8985014]
47. Pasupathy A, Miller EK. Different time courses of learning-related activity in the prefrontal cortex and striatum. Nature. 2005; 433:873–876. [PubMed: 15729344]
48. Jarvis ED. Learned birdsong and the neurobiology of human language. Ann N Y Acad Sci. 2004; 1016:749–777. [PubMed: 15313804]
49. Butler AB, Reiner A, Karten HJ. Evolution of the amniote pallium and the origins of mammalian neocortex. Ann N Y Acad Sci. 2011; 1225:14–27. [PubMed: 21534989]
50. Foster EF, Mehta RP, Bottjer SW. Axonal connections of the medial magnocellular nucleus of the anterior neostriatum in zebra finches. J Comp Neurol. 1997; 382:364–381. [PubMed: 9183699]

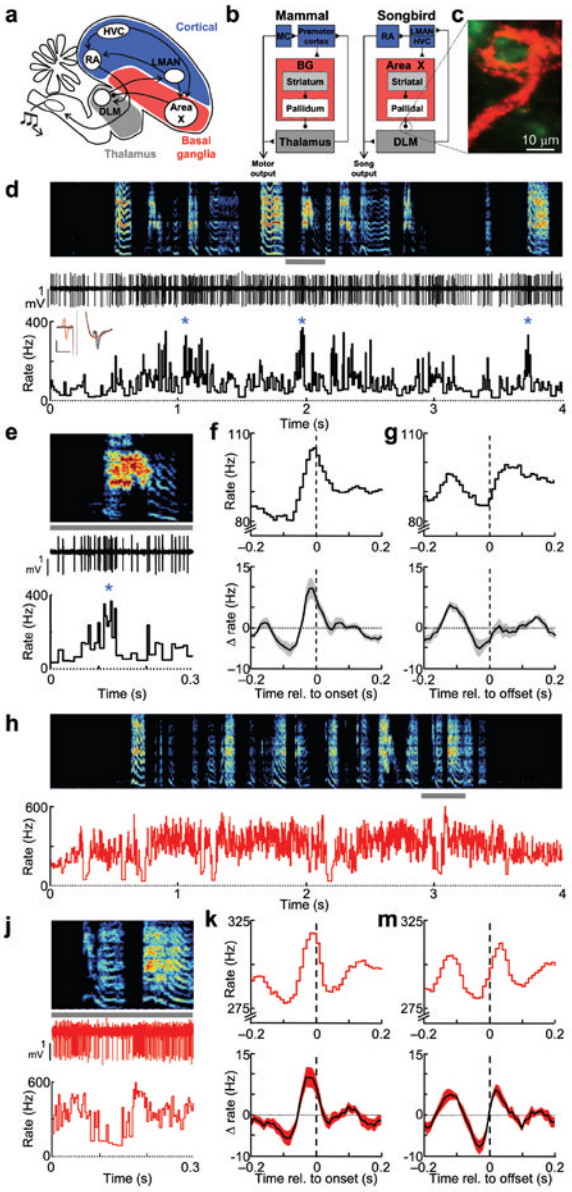

Figure 1. Firing patterns of thalamic neurons and their pallidal inputs during singing

(**a–b**) LMAN, Area X and DLM constitute 'cortical[48],' basal ganglia, and thalamic portions of the song system, respectively. LMAN contributes to vocal output through its projection to RA, a motor cortical (MC) nucleus, which in turn projects to brainstem motor neurons. Adult song production involves the HVC→RA projection. (**c**) Confocal image of a calyceal pallidal axon terminal (red) and the postsynaptic DLM neuron (green). (**d**) Extracellular voltage trace and the instantaneous firing rate of a single thalamic neuron recorded during subsong (spectrogram shown above, 44 dph). *Inset*, antidromic identification and collision testing demonstrating the projection to LMAN; evoked DLM spike following stimulation in LMAN (black trace), LMAN stimulation triggered by a spontaneously DLM elicited no antidromic spike (red trace); vertical and horizontal scale bars: 1 mV and 1 ms, respectively. (**e**) Expanded view from panel d (gray bar). (**f**) Syllable onset-aligned rate histograms for the neuron in shown in panel d (top) and for all DLM neurons (bottom, shading indicates ± s.e.m.) (n = 14) *x* axis label: Time relative to syllable onset (s). (**g**) Syllable offset-aligned

rate histogram. Data are shown as in f. (**h–m**) Data are plotted as in d–g for a pallidal axon terminal recorded in the same bird and on the same day as the DLM neuron from panel d.

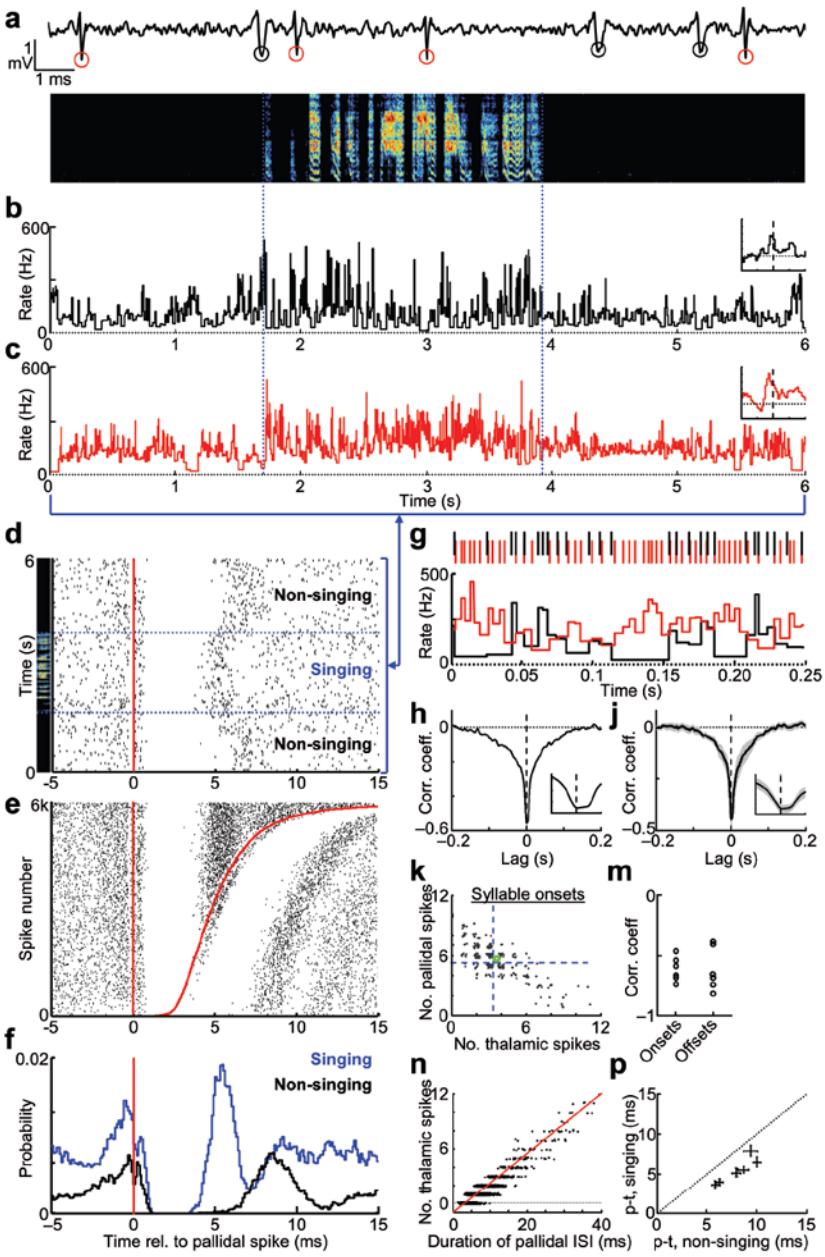

Figure 2. Simultaneous recordings of pallidal axon terminal and putative post-synaptic thalamic neurons during singing

(**a**) Extracellular waveform containing thalamic and pallidal spikes (red and black circles, respectively). (**b–c**) Instantaneous firing rates of the thalamic and pallidal neurons during subsong (spectrogram above, 48 dph). *Insets*, syllable onset-aligned rate histograms, plotted as in Fig. 1g, *x* axis: ± 0.2 s relative to syllable onset; *y* axis: Δ Rate: −10 to 25 Hz. (**d**) Raster plot of thalamic spikes (black ticks) aligned to the timing of pallidal spikes (red line) for the data shown in panels b–c. (**e**) Raster plot, as in d, sorted by the duration of the pallidal interspike interval (ISI) during singing. Red line at right shows the time of the next pallidal spike (6,000 pallidal ISIs shown). (**f**) Histograms of thalamic spike probability relative to pallidal spike times. (**g**) Zoom in of panels b-c (*), showing anti-correlation of pallidal (red) and thalamic (black) instantaneous firing rates (IFR). (**h**) Lag cross-correlation

of the firing rates (same pair). *Inset*, expanded view of the negative peak of the cross correlation (± 10 ms). (**j**) Average lag cross-correlation of 6 pairs (shading, ± s.e.m). (**k**) Scatter plot of the number of pallidal spikes vs. thalamic spikes that occurred in a 30 ms window prior to each syllable onset (255 syllables, same pair as panels b-c). Green circle indicates mean number of spikes in this window. Blue dashed lines indicate average number of pallidal and thalamic spikes in random 30 ms windows during singing. (**m**) Correlation, for all six pairs, between of the number of pallidal and thalamic spikes occurring in the 30 ms preceding syllable onsets and offsets. (**n**) The number of thalamic spikes within each pallidal ISI, plotted as a function of ISI duration (red line, linear regression; pair from panels b-c). (**p**) Average duration of DLM spike suppression, singing versus non-singing (± s.d., n = 6 pairs).

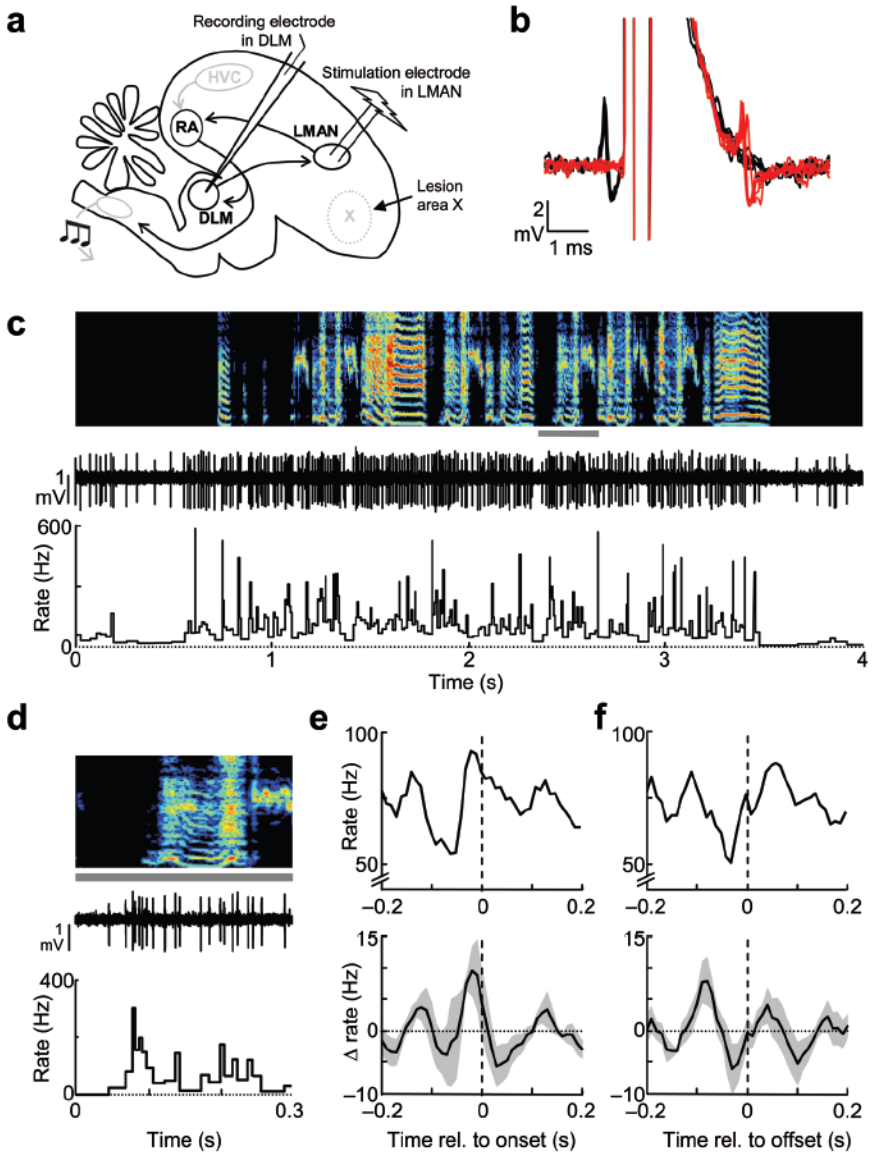

Figure 3. Song-locked rate modulations in DLM neurons are also observed after Area X lesions

(**a**) Schematic of experimental design of recording and stimulation electrodes in DLM and LMAN, and of lesion of Area X (see Methods). (**b**) Antidromic identification and collision testing of an LMAN-projecting neuron in DLM. (**c**) Extracellular voltage trace and instantaneous firing rate of the same DLM neuron (shown in b) recorded during singing (spectrogram shown above). (**d**) Example of spiking of the DLM neuron at a syllable onset: data are an expanded view from the period marked by a gray bar in panel c. (**e**) Syllable onset-aligned rate histograms for the same neuron (top), and for all DLM neurons recorded in Area X-lesioned birds (bottom, n = 6 neurons from 3 birds). Note that the apparent rate change in the population histogram was less than that measured across neurons because the peak prior to syllable onsets occurred at slightly different times in different neurons. (**f**) Syllable offset aligned rate histograms; data shown as in e.

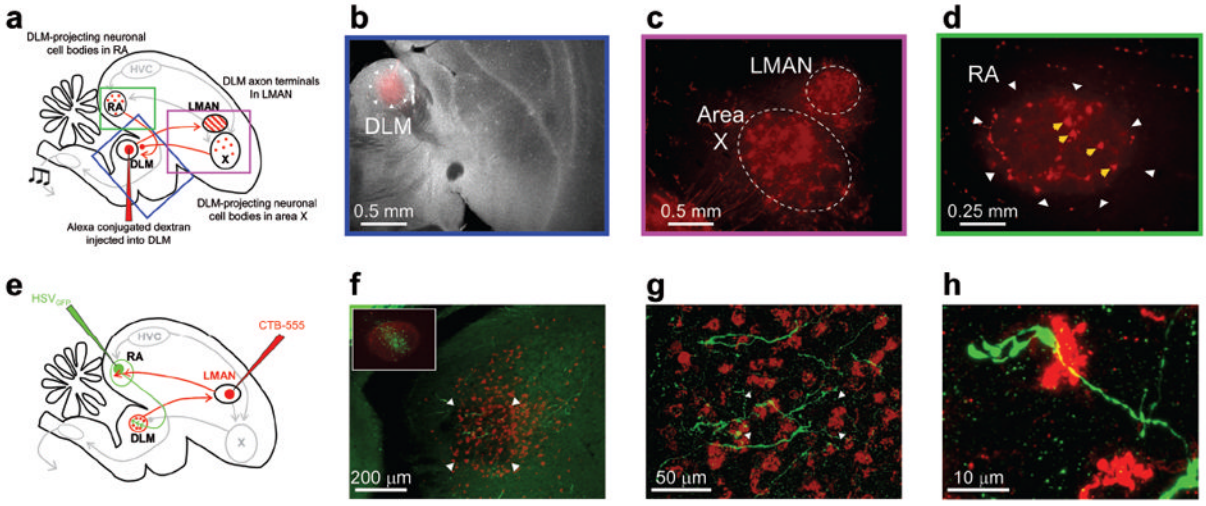

Figure 4. Anatomical verification of the RA projection to DLM in juvenile birds

(**a**) Schematic of retrograde identification of DLM-projecting RA neurons. Boxes highlight expanded views shown in panels b–d. (**b**) Merged darkfield-fluorescence section showing Alexa-555 conjugated dextran injected into the vocal portion of DLM in a juvenile bird (37 dph). (**c**) Retrograde labeling of cell bodies in Area X and axon terminals in LMAN, confirming the placement of tracer into the vocal portion of DLM. (**d**) Following injection of tracer into DLM, cell bodies were also labeled in RA (yellow arrows). (**e**) Schematic of anterograde identification of RA axon terminals in DLM. (**f**) Micrograph of DLM, showing neurons retrogradely labeled (red) by injection of tracer into LMAN. RA axon terminals, green, were labeled by injection of GFP-expressing HSV virus into RA. *Inset*, Micrograph of RA, showing anterograde label of LMAN axon terminals (red), and GFP expressing neurons (green). (**g**) Expanded view micrograph in DLM showing RA terminals, from the region marked by the arrowheads in f. (**h**) Expanded view in DLM showing RA terminals in DLM, from the region marked by the arrowheads in g.

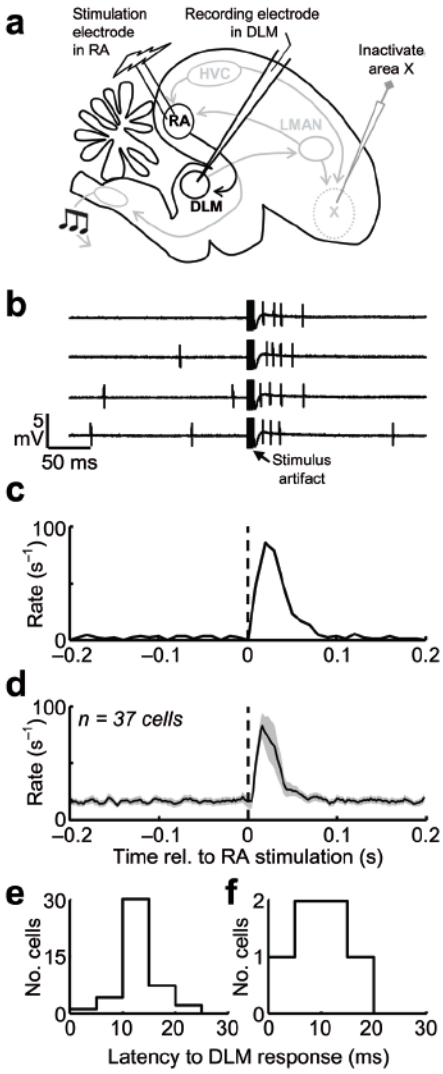

Figure 5. RA stimulation activates DLM neurons

(**a**) Schematic of the experimental design. DLM neurons were recorded in anesthetized birds during inactivation of Area X[19] (see Supplementary Fig. 9). (**b**) Four example traces of a DLM neuron recorded during burst stimulation of RA (5 stimulations at 500 Hz). Note the increase in DLM firing rate immediately following RA stimulation. Single-pulse stimulation of RA was also effective in driving DLM neurons (see Supplementary Fig. 9). (**c**) RA-stimulation-aligned rate histogram for the neuron shown in b. (**d**) Average peristimulus histogram for 37 neurons recorded in 9 birds (shading indicates ± s.e.m.). (**e**) Histogram of response latencies of DLM neurons following RA burst stimulation (n = 37 neurons). (**f**) Histogram of response latencies in DLM following single-pulse stimulation in RA.

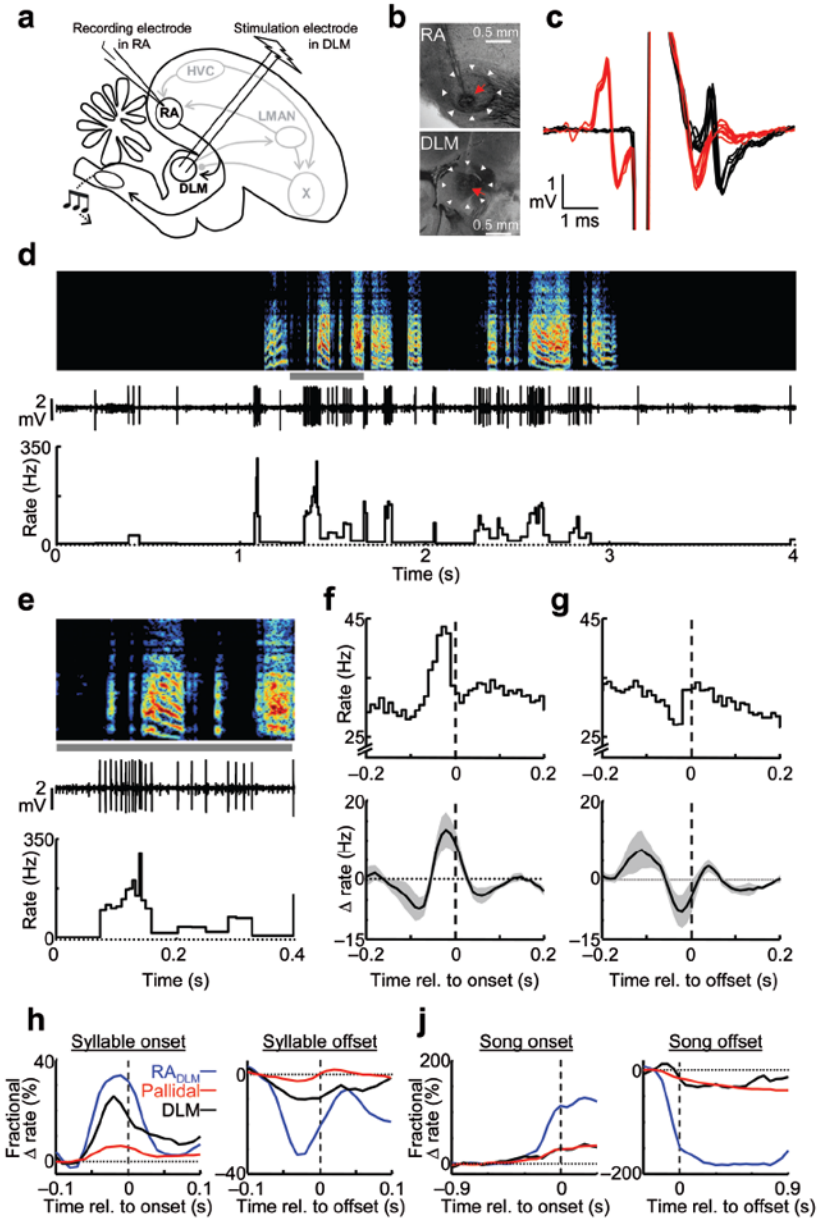

Figure 6. Singing-related firing patterns of RA neurons projecting to DLM

(**a**) Schematic of experimental design. (**b**) Histological verification of recording and stimulation electrodes in RA and DLM. (**c**) Antidromic identification and collision testing of a DLM-projecting neuron in RA. (**d**) Extracellular voltage trace and instantaneous firing rate of the same RA_{DLM} neuron (shown in c) recorded during singing (spectrogram shown above, 46 dph). (**e**) Example of spiking of an RA_{DLM} neuron at syllable onsets, from the period marked by a gray bar in panel d. (**f**) Syllable onset-aligned rate histograms for the same neuron (top), and for all RA_{DLM} neurons (bottom, n = 17). (**g**) Syllable offset-aligned rate histograms; data shown as in g. (**h**) Average fractional rate change (Δ rate divided by the mean baseline rate) for RA_{DLM} neurons (n = 17, blue), pallidal terminals (n = 14, red), and DLM neurons (n = 14, black) aligned to syllable onsets (left) and offsets (right). (**j**) Average fractional rate changes, plotted as in panel h, aligned to the onset of singing (left) and offset of singing (right).